Electronic Supplementary Material (ESI) for Physical Chemistry Chemical Physics.

Carrier dynamics in highly-excited $TlInS_2$: Evidence of 2D electron-hole charge separation at parallel layers

Vytautas Grivickas, *[a] Patrik Ščajev,[a] Vitalijus Bikbajevas,[a] Olga V. Korolik,[b] and Alexander V. Mazanik[b]

[a] Institute of Photonics and Nanotechnology, Vilnius University, Saulėtekio av. 3, 10257 Vilnius, Lithuania

[b] Energy Physics Department, Belarusian State University, Nezavisimosti av. 4, 220030 Minsk, Republic of Belarus

Supporting information

SI. 1. Micro-Raman measurements

Micro-Raman spectra were recorded with Nanofinder HE apparatus (*LOTIS-TII,* Belarus – Japan), the confocal spectrometer equipped with a 3D piezo-scanning system. The 532 nm or 473 nm CW DPSS laser was used as an excitation source. Optical power incident on the samples was reduced down to 200 μW to avoid their damage. The 50x objective lens (NA = 0.8) provided size of excitation spot of about 0.7 μm. Spectral resolution and accuracy of Raman shift is depending on the used diffraction grating which was better than 2.5 cm^{-1} or 0.8 cm^{-1} (Fig. S1). The Raman signal originated from depth about 2 μm.

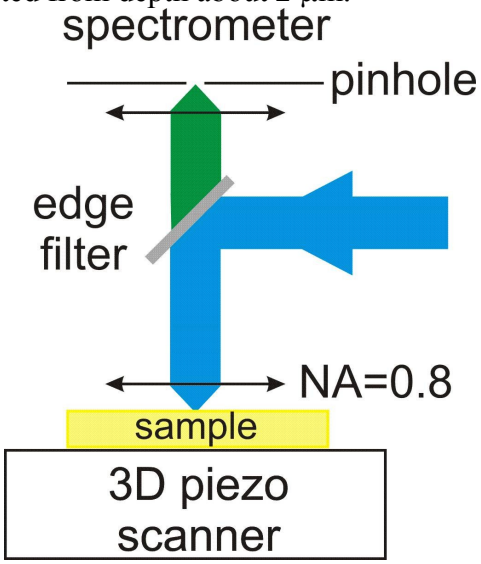

Figure S1. Optical layout of the confocal micro-Raman spectroscopy.

Fig. 2 demonstrates typical Raman spectra of the undoped (pristine) and the Er-doped $TlInS_2$ without any external pulse irradiations. The main Raman lines and shoulder fingerprints are indicated. The lines above 100 cm^{-1} can be assigned to optical vibrations of the rigid In_4S_{10} groups of the A_g symmetry. Their intensities and ratios are in good agreement with room temperature data published in Refs. [28,29]. Figure demonstrates that incorporation of *Erbium* does not change the composition of the layered crystal structure vibrations as well as phonon energies.

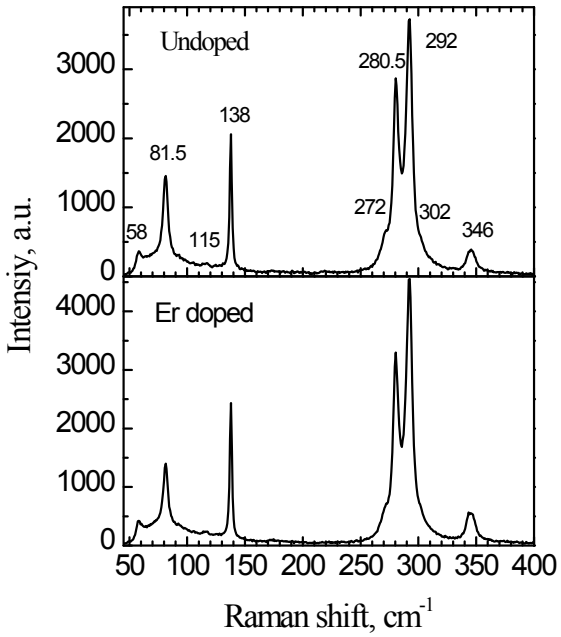

Figure S2. Unpolarized Raman spectra of the pristine and the *Erbium* doped $TlInS_2$ crystals as excited by 532 nm laser at k||c and measured in the backwards direction. The spectral resolution is 0.8 cm^{-1}. Typical line frequencies and shoulder fingerprints are indicated. The range under 55 cm^{-1} is damped by an notch filter.

Fig. S3 demonstrates Raman spectra at two points of irradiated $TlInS_2$ crystals after TG period of $\Lambda = 8$ μm. The points are separated by a half-period distance. As can be seen, the phase created by intense light pulse has the following peculiarities (i) the wide background plateau, (ii) the broadening of the main Raman line doublet at 280.5 cm^{-1} and 292 cm^{-1}, (iii) the splitting a weak Raman line at 246 cm^{-1}, and (iv) the disappearance of the acoustic Raman line at 81 cm^{-1}. We observe interesting trend. The broadening of the Raman background varies with period as $\Lambda/4$ while the broadening of doublet at 280.5 cm^{-1} and 292 cm^{-1} varies with period of $\Lambda/2$ in the coordinate position (see Fig. 10 of the main text). The presented features testify the transition into two different crystal phases takes place in corresponding points. The depth resolve Raman shows that such phases persist in depth sufficiently above 5 μm. The pristine and the Er doped crystal $TlInS_2$ are identical in Fig. S3 (a,c) and Fig. S3 (b,d), meaning that both crystal types behave in the same way. This indicates that PSFs frequency, which is introduced and discussed in the main text as major factor providing PL intensity, has minor importance for imprinted phases.

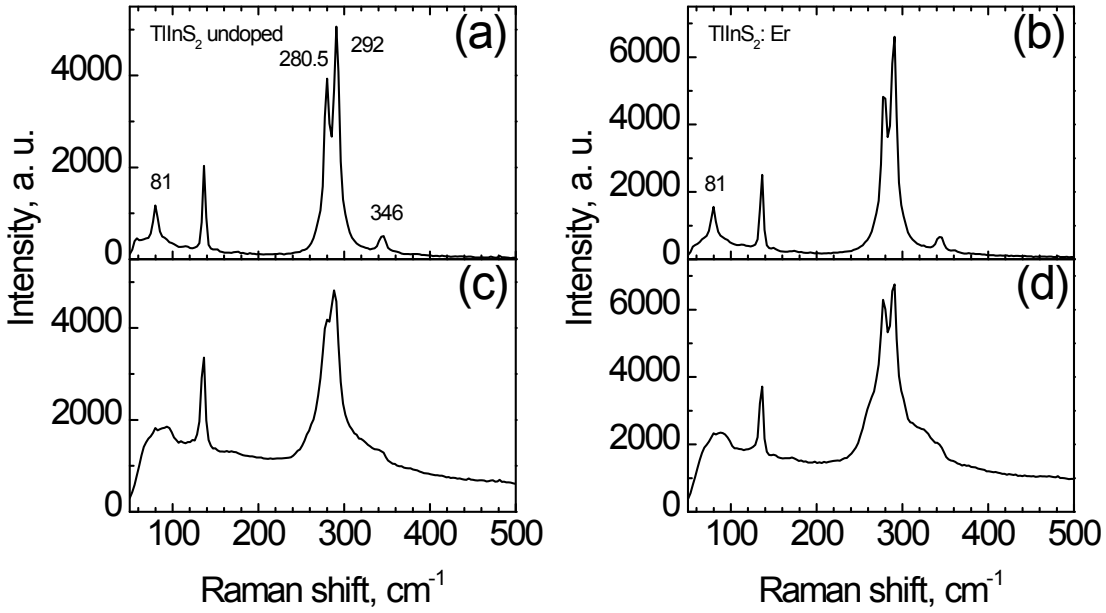

Figure S3. Raman spectra for pristine (a,c) and Er doped (b,d) $TlInS_2$ crystals after TG image irradiation in the two points (upper in less irradiated and bottom in strongly irradiated fringe) separated by a half-period distance (Λ = 8 μm). The resolution is 1.2 cm^{-1}, the excitation wavelength is 532 nm.

SI. 2. Time-resolved PL measurements

Fig. S4 (a) presents PL decays in $TlInS_2$(Er) sample at various wavelengths of the emitting band. It can be noted a similar decay character with an exponetial slope expressed at the beginning of the decay. This invariant indicates that all radiation wavelengths obey by same intrisic emission mechanism which we accounted to be a phonon-assisted radiative exciton dipoles oriented in direction out-of-plane at RT. In untreated $TlInS_2$ samples doped by *Erbium* the PL intensity in particular excitation spot varies in the ranges of about 20% and the internal quantum efficiency is estimated to be within 1-2%. In the pristine $TlInS_2$ samples this spread is statistically higher (~50-70%) showing a lower quality of this crystal due to more frequent PSF distributions between the layers as disscused in the main text. Similar satatistical variation was observed by SPL (see Ref. [9], main text).

Fig. S4 (b) presents high energy part in the emission spetra on the log intensity scale. The exponential slope is identified by lines. The slope dependence is fitted by straight lines providing value of the electron-hole gas temperature (see Fig. 4 b). Similar T_{eh} values have been obtained in the pristine $TlInS_2$ crystal after TP generation (not presented).

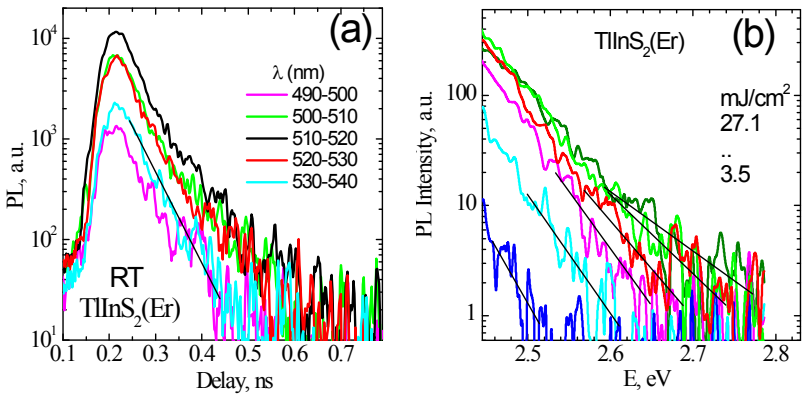

Figure S4. (a) The PL decay at different emitted wavelengths in $TlInS_2$(Er) crystal after TP generation. (b) A part of the high PL energy region fitted by Eq. (4). The corresponding *e-h* gas temperatures T_{eh} are determined (see main text, Fig. 4 b).

SI. 3. TG measurements

Fig. S5 shows diffraction efficiency decay in the pristine $TlInS_2$ at different fluences (a) and corresponding DE dependence on excitation fluence at $\Delta t = 0$ and $\Delta t = 2.4$ ns (b). While at $\Delta t = 0$ the DE magnitude exceeds the one for $\Delta t = 2.4$ ns by two orders, no saturation obviously occurs on the slower part. This can be hardly attributed to simple trapping effect when excited carrier concentration exceeds density of the corresponding trap. The gradual character in the excitation dependence at $\Delta t = 2.4$ ns implies carrier access to the recombination sink controlled by diffusion parameter (stretched exponential component in Fig. 8).

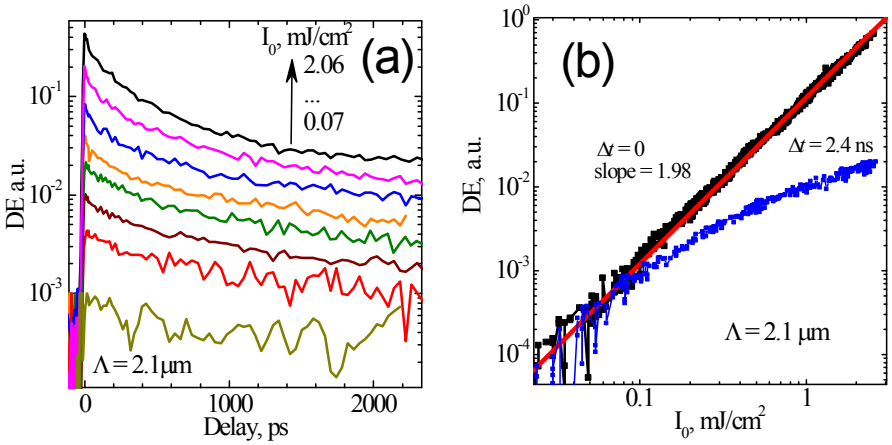

Figure S5. (a) Diffraction efficiency decay in the pristine $TlInS_2$ at $\Lambda_2 = 2.1$ μm for different pulse fluences and (b) DE magnitude *vs* pump fluence at $\Delta t = 0$ and $\Delta t = 2.4$ ns.

Fig. S6 demonstrates that, in the *Erbium* doped $TlInS_2$ crystal, normalized radiative decay take place at the rate in two times faster than nonradiative recombination kinetics obtained by TG. This behavior suggests the bipolar mechanism of recombination between electrons and holes.

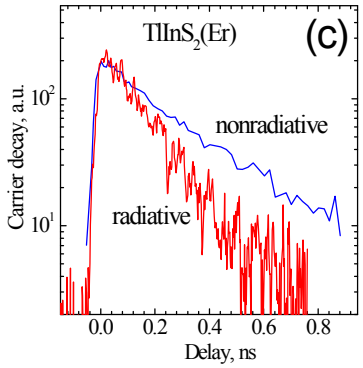

Figure S6. Normalized radiative and nonradiative decay in $TlInS_2$: Er doped crystal. The PL decay occurs twice faster than the nonradiative one. This behavior is expected for bipolar radiation of excess *e-h* pairs [39].

SI. 4. Calculation of carrier diffusion length along the layers

Ignoring vertical diffusion across the layers as being very slow process, a simple modeling through consideration the 1D-diffusion to the recombination sinks at PSF edges can be applied. The process can be described by following diffusion equation:

$$\frac{\partial \Delta N(x,t)}{\partial t} = D_{\|} \frac{\partial^2 \Delta N(x,t)}{\partial x^2} - \frac{\Delta N(x,t)}{\tau_{bulk}} \qquad \text{(S1)}$$

with boundary conditions

$$D_{\|} \frac{\partial \Delta N(x,t)}{\partial x}\bigg|_{x=0} = S_1 \Delta N(0,t)$$
$$D_{\|} \frac{\partial \Delta N(x,t)}{\partial x}\bigg|_{x=L} = -S_2 \Delta N(L,t) \qquad \text{(S2)}$$

Here $D_{\|}$ is the ambipolar diffusivity along the layer, S_1 and S_2 are recombination rates at PSF edges separated by distance L in x-coordinate, and τ_{bulk} is the bulk carrier lifetime. For an exponential decay the effective lifetime can be written as $\tau^{-1} = \tau_{bulk}^{-1} + \tau_s^{-1}$ where the second term reflects the sink recombination. Its influence can be evaluated by solving Eq. (S1) for a main mode. A useful approximation of this solution was obtained by consideration two limiting cases for $S \to 0$ and $S \to \infty$ [1-3]. The maximum deviation of the approximation from an exact numerical solution of Eq. (S1) does not exceed 5%. Then, the approximation of τ_s takes quite simple form

$$\tau_s = \frac{(BL)^2}{\pi^2 D_{\|}} + \frac{L}{S_1 + S_2}, \qquad \text{(S3)}$$

Here we have included the parameter B; $1 \le B \le 2$. This asymmetry parameter describes carrier distribution in the layer. Asymmetry occurs if one S value is smaller than another or if a distance between the transient grating fringes is larger/smaller than the L, see details in Refs. [3]. The first term in Eq. (S3) reflects the pure diffusive component (for large S values) and the second - the pure sink recombination component (for small S values). The slower one of two processes will be the rate limiting process and will dominate in τ_s. Since in our experiments the injection dependence of excess carrier concentration exhibits an inverse correlation between D and lifetime, we consequently assume that diffusion controls the lifetime and we neglect the second term in Eq. (S3). Inserting the measured lifetime and diffusion injection dependences from fits of Fig. 7 (a,b) in the main text and assuming that the contribution of the τ_{bulk} is negligibly small (τ_{bulk} is of the order of μs), we determined from Eq. (S3) the length L in the two types of $TlInS_2$ crystals. The result is shown in Figure S7. The diffusion length is about 0.7 μm, almost injection level independent, quite similar in both types of investigated $TlInS_2$ crystals. Some deviation for the pristine sample can be attributed by lager inhomogeneity of parameters (see Fig. 7 in the main text).

As the first terms in Eq. (S3) always is larger than the second one, inserting obtained L value from inequality of terms we may estimate S rates which satisfy such diffusion-limiting assumption. We found that values $S_1 + S_2 >> 7\times10^4$ cm/s would fit a resulting regime. Such S values are quite typical to disordered interfaces which contain active sites in ionic semiconductor [4].

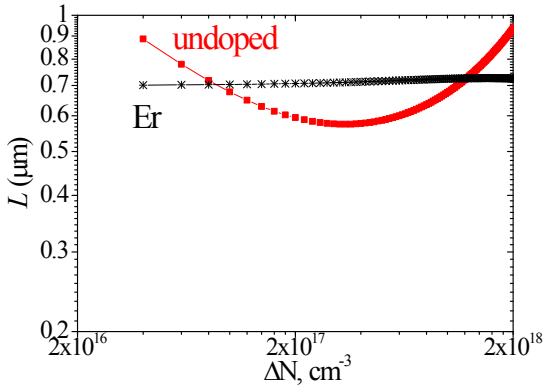

Fig. S7. Carrier diffusion length calculated from TG transients as a function of injected carrier concentration in undoped and *Erbium* doped $TlInS_2$ crystals. Parameter B =2 is used in the Eq. (S3).

References

[1] V. Grivickas, J. Linnros, A. Vigelis, J. Seckus and J.A. Tellefsen, A study of carrier lifetime in silicon by laser induced absorption: a perpendicular geometry measurement, Sol. St. Electron. **35,** 299 (1992).

[2] P.B. Klein, R. Myers-Word, K.-K. Lew, B.L. VanMil, C.R. Eddy Jr., D.K. Gaskill, A. Shrivastava, and T.S. Sudarshan, Recombination processes controlling the carrier lifetime in n−4H–SiC epilayers with low Z1/2 concentrations, J. Appl. Phys. **108**, 033713 (2010).

[3] S.S. Suvanam, K. Gulbinas, M. Usman, M.K. Linnarson, D.M. Martin, J. Linnros, V. Grivickas, and A. Hallén, 4H-SiC-Dielectric Interface Recombination Analysis Using Free Carrier Absorption, J. Appl. Phys. **117,** 105309 (2015).

[4] P. Ščajev, S. Miasojedovas, A. Mekys, D. Kuciauskas, K.G. Lynn, S.K. Swain, and K. Jarašiūnas, Excitation-dependent carrier lifetime and diffusion length in bulk CdTe determined by time-resolved optical pump-probe techniques, J. Appl. Phys. **123**, 025704 (2018).